Korean J. Chem. Eng., **31**(7), 1162-1167 (2014)
DOI: 10.1007/s11814-014-0010-x

pISSN: 0256-1115
eISSN: 1975-7220

CH_4 reforming with CO_2 for syngas production over nickel catalysts supported on mesoporous nanostructured γ-Al_2O_3

Nasrollah Majidian*, Narges Habibi*, and Mehran Rezaei,†**

*Faculty of Engineering, Tehran North Branch, Islamic Azad University, Tehran, Iran
**Catalyst and Advanced Materials Research Laboratory, Chemical Engineering Department, Faculty of Engineering, University of Kashan, Kashan, Iran
(*Received 28 July 2013 • accepted 7 January 2014*)

Abstract–Nanostructured γ-Al_2O_3 with high surface area and mesoporous structure was synthesized by sol-gel method and employed as catalyst support for nickel catalysts in methane reforming with carbon dioxide. The prepared samples were characterized by XRD, BET, TPR, TPH, SEM and TPO techniques. The BET analysis showed a high surface area of 204 m^2g^{-1} and a narrow pore-size distribution centered at a diameter of 5.5 nm for catalyst support. The results revealed that an increase in nickel loading from 5 to 15 wt% decreased the surface area of catalyst from 182 to 160 m^2g^{-1}. In addition, the catalytic results showed an increase in methane conversion with increase in nickel content. TPO analysis revealed that the coke deposition increased with increasing in nickel loading, and the catalyst with 15 wt% of nickel showed the highest degree of carbon formation. SEM and TPH analyses confirmed the formation of whisker type carbon over the spent catalysts. Increasing CO_2/CH_4 ratio increased the methane conversion. The BET analysis of spent catalysts indicated that the mesoporous structure of catalysts still remained after reaction.

Keywords: Nanostructured, γ-Al_2O_3, Nickel Catalyst, Dry Reforming, Syngas

INTRODUCTION

CO_2 reforming of methane shows a growing interest from both industrial and environmental viewpoints. From an environmental viewpoint, CO_2 and CH_4 are undesirable greenhouse gases and both are consumed by this reaction. One potential advantage of dry reforming that would have an impact on the industrial sector is the lower H_2 : CO product ratio that can be produced, i.e., 1 : 1 or less. A lower H_2 : CO ratio is preferred for the production of oxygenated compounds [1-4]. The major drawback of this reaction, however, is the rapid deactivation caused by carbon deposition via the Boudouard reaction ($2CO \leftrightarrow C+CO_2$) and/or CH_4 decomposition. Many efforts have focused on development of metal catalysts, which bear high catalytic performance towards synthesis gas formation, and are also resistant to carbon deposition, thus displaying stable long-term operation. Noble metal catalysts are less sensitive to carbon deposition [5,6]. However, transition metals, such as Ni, Fe and Co, are often preferred, considering the high cost and limited availability of noble metals. Among these metals nickel might be the optimum active component of the potential catalyst designed [2,4]. Usually, Ni has been supported on different carriers such as MgO, Al_2O_3, promoted Al_2O_3, TiO_2, CeO_2, etc. However, it tends to deactivate by coke formation and sintering of nickel particles [2,7], which is closely related to the catalyst structure and composition. Among these supports, Al_2O_3 has a high potential as a catalyst support [4,8,9]. The use of alumina requires a high specific surface area and suitable pore structure for catalysis applications. In this paper, mesoporous nanocrystalline γ-Al_2O_3 with high surface was prepared and employed as catalyst support for nickel catalyst in dry reforming.

EXPERIMENTAL

1. Preparation of Ni/Al_2O_3 Catalysts

Ni/Al_2O_3 catalysts with different Ni contents were prepared by impregnation method. The catalyst support was prepared by sol-gel method. Aluminum tri isopropylate (98% purity, Merck) was first hydrolyzed in distillated water by stirring for 1 hour at 80-85 °C. Subsequently, HNO_3 was added dropwise with HNO_3 to Al molar ratio of 1/1 and refluxed for 12 h at 98 °C. The sol was then kept for 2 h at 98 °C in air atmosphere without refluxing. After this step the sol became very viscous. The formed gel was dried at 80 °C and calcined at 700 °C. After preparation of catalyst support, a certain amount of $Ni(NO_3)_2 \cdot 6H_2O$ was dissolved in distilled water under stirring and then the dehydrated catalyst support was added to nickel nitrate solution under stirring for 2 h at room temperature. The suspension was dried at 80 °C for 10 h and calcined at 500 °C for 4 h with heating rate of 3 °C·min^{-1}.

2. Characterization

X-ray diffraction (XRD) analysis was performed using an X-ray diffractometer (PANalytical X'Pert-Pro) with a Cu-Kα monochromatized radiation source and an Ni filter in the range 2θ=10-70° to examine the crystallinity of the prepared samples.

The N_2 adsorption-desorption analysis was at boiling temperature of nitrogen (−196 °C) using an automated gas adsorption analyzer (Tristar 3020, Micromeritics). The samples were purged with nitrogen gas for 2 h at 250 °C using VacPrep 061 degas system (Micromeritics). Temperature programmed reduction (TPR) analysis was used for evaluating the reduction properties of prepared catalysts with

†To whom correspondence should be addressed.
E-mail: rezaei@kashanu.ac.ir

Micrometrics chemisorb 2750 instrument. In the TPR measurement, 100 mg catalyst was subjected to a heat treatment (10 °C/min) in a gas flow (30 ml/min) containing a mixture of H_2 : Ar (10 : 90). Prior to TPR experiment, the samples were heat treated under an inert atmosphere (Ar) at 250 °C for 1 h. The H_2 uptake amount during the reduction was measured with a thermal conductivity detector (TCD).

Temperature programmed oxidation (TPO) of spent catalysts was performed in a similar apparatus by introducing a gas flow (20 ml/min) of the mixture O_2/He (5 : 95) over 25 mg of spent catalysts, and the temperature was increased with a heating rate of 10 °C/min up to 800 °C. Temperature programmed hydrogenation (TPH) of spent catalysts was in the same apparatus as described for TPR. The spent catalyst (about 25 mg) was submitted to a heat treatment (10 °C/min up to 800 °C) in a gas flow (30 ml/min) of the mixture H_2 : Ar (10 : 90).

3. Catalytic Activity Measurement

Activity measurements were carried out in a fixed-bed continuous-flow reactor made of a 7-mm-i.d. quartz tube at atmospheric pressure. The reactor was loaded with 200 mg of the prepared catalyst. Prior to the reaction, the catalysts were reduced in a H_2 gas flow of 20 mL·min^{-1} at 700 °C for 4 h. The reactant gas feed consisted of CH_4 and CO_2 was introduced into the reactor and the activity tests were performed at different temperatures, ranging from 550 to 700 °C in steps of 50 °C. The loss in catalyst activity at 700 °C was monitored up to 5 h time on stream. The gas composition was analyzed by a HID YL-6100 gas chromatograph equipped with a carboxen1010 column.

RESULTS AND DISCUSSION

X-ray diffraction was used to identify crystalline phases in the prepared catalysts and to obtain an indication of NiO particle size. XRD patterns of the catalyst support, as well as the prepared catalysts with different nickel contents, are shown in Fig. 1. The results revealed that the catalyst support has γ-Al_2O_3 crystalline structure. The 5% Ni/Al_2O_3 catalyst showed two major crystallite phases: γ-Al_2O_3 and nickel aluminate ($NiAl_2O_4$). γ-Al_2O_3 has a pseudospinel structure and its lattice parameters are very close to that of nickel aluminate [10], so the identification of these phases is difficult due to peak overlapping. Peaks related to NiO were not observed on the 5% Ni/Al_2O_3, due to low content and high dispersion of NiO over the catalyst support. The catalysts with higher contents of nickel (10 and 15% Ni/Al_2O_3) presented also the formation of nickel oxide (NiO). It is well known that at low content of active metal, nickel species interact with tetrahedral coordinated sites of γ-Al_2O_3, while at high nickel loadings the alumina is saturated with nickel and bulk NiO is formed on the Al_2O_3 surface. NiO particles in high NiO content tend to aggregate just as bulk NiO due to the weak interaction with alumina [11]. The XRD results clearly showed that increasing in nickel loading increased the intensity of peaks related to NiO, an indication of an increase in NiO crystallite size.

The average crystallite size of catalyst support was estimated using the Debye-Scherrer equation:

$$D = \frac{0.9\lambda}{\beta\cos\theta} \quad (1)$$

λ is the X-ray wavelength (Cu Kα), θ the Bragg angle, β the pure

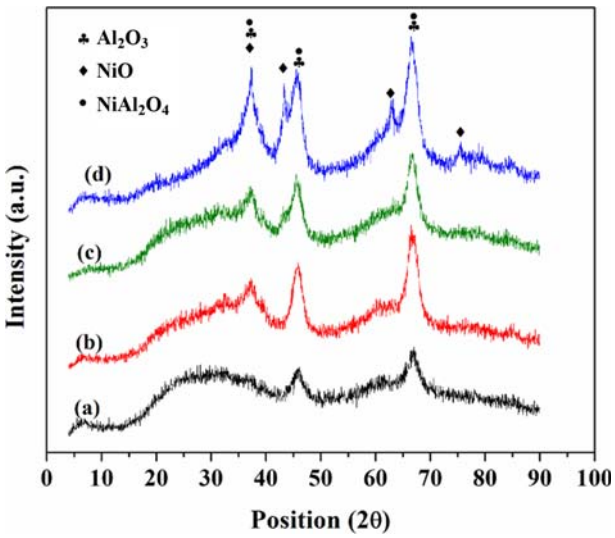

Fig. 1. XRD patterns of calcined catalysts, (a) Al_2O_3, (b) 5%Ni/Al_2O_3, (c) 10%Ni/Al_2O_3 and (d) 15%Ni/Al_2O_3.

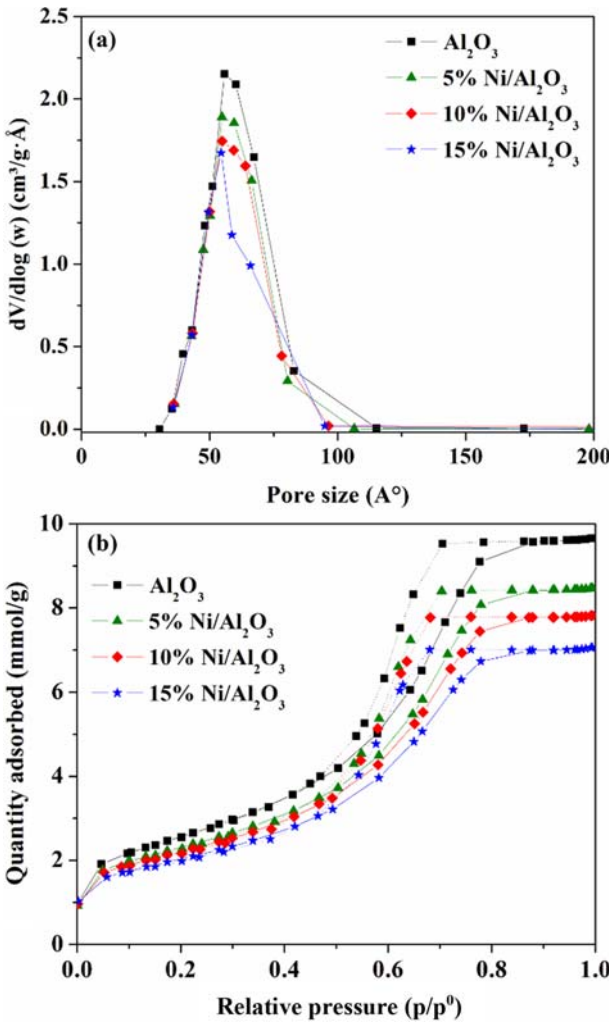

Fig. 2. (a) Pore size distributions and (b) N_2 adsorption/desorption isotherms of calcined catalysts.

Table 1. Structural properties of prepared catalysts

Catalyst	BET ($m^2 g^{-1}$) Calcined catalyst	BET ($m^2 g^{-1}$) Spent catalyst	Pore volume ($cm^3 g^{-1}$) Calcined catalyst	Pore volume ($cm^3 g^{-1}$) Spent catalyst	Pore size (nm) Calcined catalyst	Pore size (nm) Spent catalyst
Al_2O_3	204.4	-	0.410	-	5.3	-
5% Ni/Al_2O_3	182.8	150.7	0.361	0.355	5.2	6.2
10% Ni/Al_2O_3	174.4	140	0.336	0.341	5.1	6.7
15% Ni/Al_2O_3	160.7	114.3	0.305	0.297	5	7.7

full width of the diffraction line at half the maximum intensity. The results showed an average crystallite size about 7.9 nm for γ-Al_2O_3.

The pore size distributions and N_2 adsorption/desorption isotherms of the samples show that all the samples have mesoporous structure (Fig. 2(a)). It is seen that the catalyst support (γ-Al_2O_3) has a mesoporous structure with a narrow pore size distribution between 3-11 nm with a maximum cantered at 5.5 nm. The results showed that all catalysts showed a mesoporous structure, and with increasing in nickel content the pore size distribution shifted to smaller values. The nitrogen adsorption/desorption isotherms (Fig. 2(b)) can be classified as a type IV isotherm, typical of mesoporous materials and the H_2 hysteresis loop, which means solids consist of particles crossed by nearly cylindrical channels or made by aggregates (consolidated) or agglomerates (unconsolidated) of spherical particles.

The structural properties of catalyst support and catalysts with different nickel contents are presented in Table 1. γ-Al_2O_3 as catalyst support shows a high specific surface area. It can be seen that increasing Ni loading decreased the surface area and pore volume. The decrease in specific surface area and pore volume may be caused by a partial blockage of the Al_2O_3 pores by nickel oxide clusters and/or a partial collapse of the mesoporous structure. In addition, the BET results showed a decrease in pore size of catalysts by increasing nickel loading. The lowest specific surface area was observed for the catalyst with 15 wt% of Ni.

Temperature programmed reduction (TPR) with H_2 was performed to investigate the reducibility of the catalysts with different nickel loadings. The H_2-TPR profiles of calcined catalysts are shown in Fig. 3. Depending on nickel content, different peaks are observed.

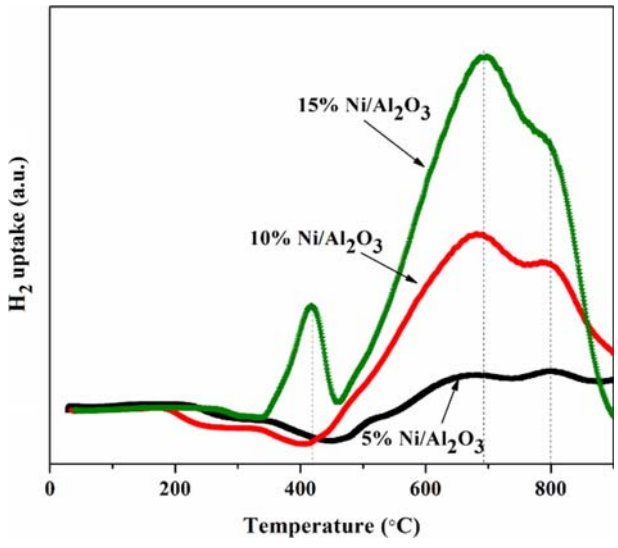

Fig. 3. TPR profiles of catalysts with different nickel contents.

For catalyst with 5 wt% of nickel a small reduction peak at about 500 °C was attributed to reduction of NiO with weak interaction with Al_2O_3.

The reduction peak around 650 °C was related to reduction of NiO with stronger interaction with catalyst support. The third small high temperature peak at around 800 °C could be related to reduction of $NiAl_2O_4$. With increasing in nickel loading, the intensity of reduction peaks increased, which is related to higher concentration of NiO in these catalysts. For the catalyst with 15 wt% Ni, a fraction of NiO was reduced at 420 °C, which is related to NiO with low interaction with catalyst support (bulk NiO), as confirmed by XRD analysis. It is well known that increasing in nickel loading decreased the nickel dispersion and increased the nickel crystallite size. From the relationship between the Ni particle size and the results of the H_2-TPR, the larger the Ni particle sizes in the catalysts, the easier they could be reduced to metallic nickel, indicating that the metal-support interaction becomes much weaker with increasing the Ni loading.

The CH_4 and CO_2 conversions on the catalysts with various nickel loadings at different reaction temperatures are shown in Fig. 4(a). The obtained results show an increase in CH_4 and CO_2 conversions with an increase in nickel loading. The higher activity of nickel catalyst with higher nickel content is related to higher concentration of active metal. Although the nickel dispersion decreased by increasing in nickel loading, but on the catalysts with low content of nickel a fraction of nickel oxide was transformed to $NiAl_2O_4$ and the accessible nickel for reaction decreased. So the catalyst with 5 wt% of Ni showed lower activity than that observed for the catalysts with higher nickel content. The obtained results also show that the CO_2 conversion was higher than methane conversion, which could be explained by reverse water-gas shift reaction ($CO_2+H_2 \leftrightarrow CO+H_2O$) that is occurring parallel with dry reforming reaction.

Fig. 4(b) shows the H_2 and CO yields of prepared catalysts with different nickel contents. H_2 and CO yields increased by increasing reaction temperature and nickel loading. The results show that the CO yield for all catalysts was higher than H_2 yield, indicating the occurrence of reverse water gas shift reaction.

Fig. 4(c) shows the stability of CH_4 for prepared catalysts at 700 °C. All the catalysts, except catalyst with 15 wt% of nickel, show relatively high stability during the reaction. The highest stability is observed for the catalyst with the lowest nickel content and the catalyst with 15 wt% of nickel shows a high degree of deactivation with time on stream. The same trend was also observed for the stability of CO_2 (Fig. 4(d)). The BET analysis revealed that the specific surface area of spent catalysts decreased after reaction and the highest decrease of surface area was observed for the catalyst with 15 wt% of Ni (Table 1). In addition an increase in pore size of spent catalysts was observed compared to calcined catalysts.

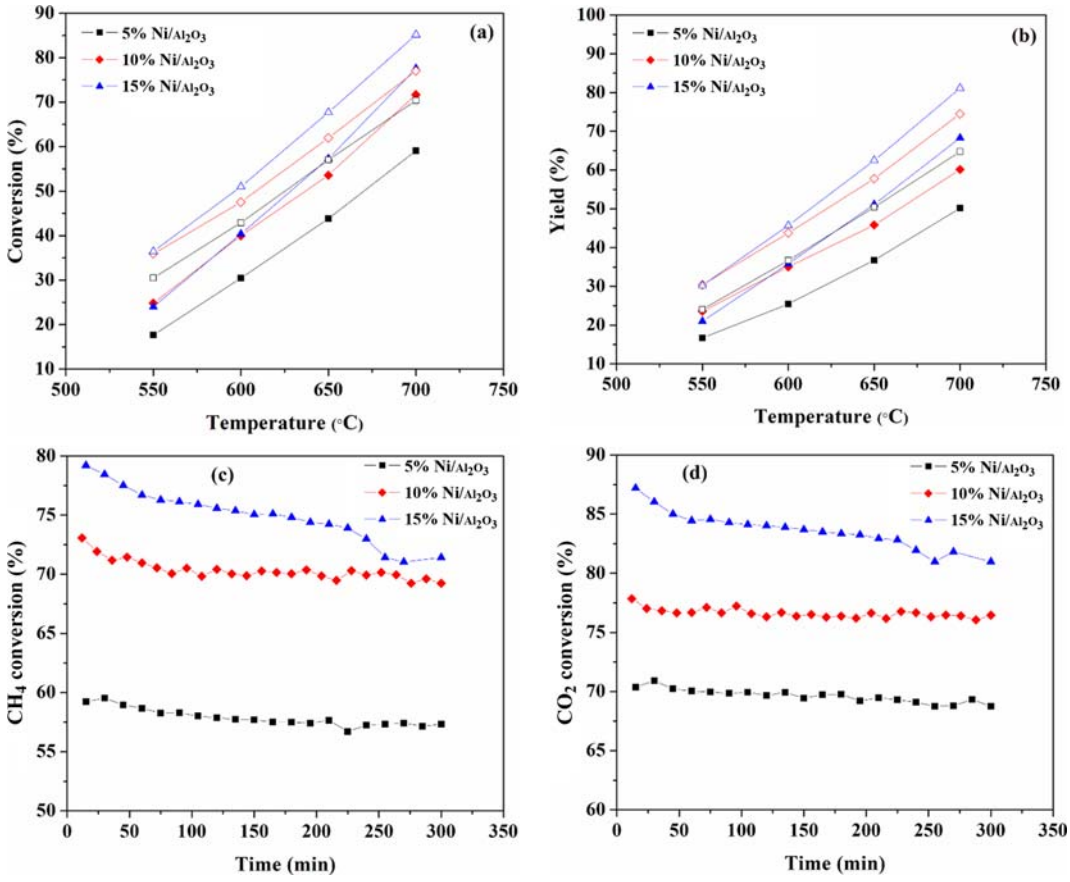

Fig. 4. (a) CH_4 (filled symbol) and CO_2 conversions (unfilled symbol), (b) H_2 yield (filled symbol) and CO yield (unfilled symbol), (c) CH_4 stability and (d) CO_2 stability of prepared catalysts at 700 °C, CO_2/CH_4=1, GHSV=18,000 ml/g_{cat}·h.

The pore size distributions and N_2 adsorption/desorption isotherms of the spent catalysts are shown in Fig. 5(a) and 5(b), respectively. Fig. 4(a) shows that the mesoporosity remained after reaction. In addition, the nitrogen adsorption/desorption isotherms (Fig. 5(b)) can be classified as a type IV isotherm, typical of mesoporous materials and the H_2 hysteresis loop.

Deactivation of nickel catalysts is caused by carbon deposition, which arises from carbon monoxide disproportionation (1) or methane decomposition (2), the latter is being favored at high temperatures:

$$2CO \leftrightarrow C+CO_2 \quad (1)$$

$$CH_4 \leftrightarrow C+2H_2 \quad (2)$$

Carbon species formed during the reforming reaction was investigated by temperature programmed oxidation (TPO) and the results are shown in Fig. 6.

The peaks at different temperatures show the existence of different types of carbon species on the catalysts during methane reforming. The small peaks at about 100 °C on the catalysts containing 15 wt% Ni could be C_α according to Bartholomew [12] and described by Mirodatos et al. [13] as a superficial carbide. Chen and Ren [14] proposed that these species may be the active intermediate. It is in agreement with assignment to this carbon species the responsibility for the CO formation. The second peak at around 220 °C, which might be amorphous carbon on the nickel sites, while the third peak at above 600 °C, is identified as whisker carbon.

TPO profiles of the spent catalysts with various nickel loadings also showed that with an increase in nickel loading, the area and the intensity of the peaks in the TPO profiles were increased. The highest intensity and area of the peak in the TPO profile were observed for the catalysts containing 15 wt% Ni. Increase in the coke deposition on the catalysts with higher nickel loadings could be related to the lower dispersion of nickel.

In addition, SEM analysis (Fig. 7) clearly showed an increase in amount of deposited carbon over the spent catalysts with higher nickel loadings. As can be seen, whisker type carbon was deposited over the spent catalysts. These results confirmed the results obtained from TPO analysis (Fig. 6).

The TPH profiles (Fig. 8) of the spent catalysts clearly show the existence of several types of carbon species on the catalysts during methane reforming.

Generally, carbon deposition is comprised of various forms of carbons, which are different in terms of reactivity. The distribution and features of these carbonaceous species depend on the nature of active metals and the composition of feed. As mentioned in the TPO analysis, these carbonaceous species can be described as completely dehydrogenated carbidic C_α type, partially dehydrogenated CH_x ($1 \leq x \leq 3$) species, namely C_β type (amorphous carbon), and carbidic clusters C_γ type formed by the agglomeration and conversion of C_α and C_β species under certain conditions. A fraction of the surface carbon species, which might be assigned to carbidic C_α, was mainly

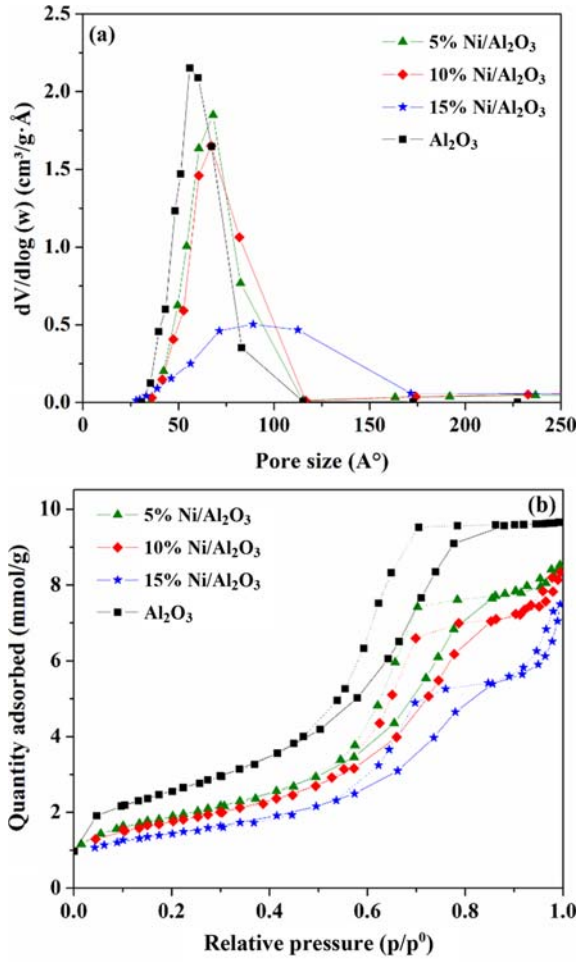

Fig. 5. (a) Pore size distributions and (b) N_2 adsorption/desorption isotherms of spent catalysts at 700 °C, CO_2/CH_4=1, GHSV= 18,000 ml/g_{cat}·h.

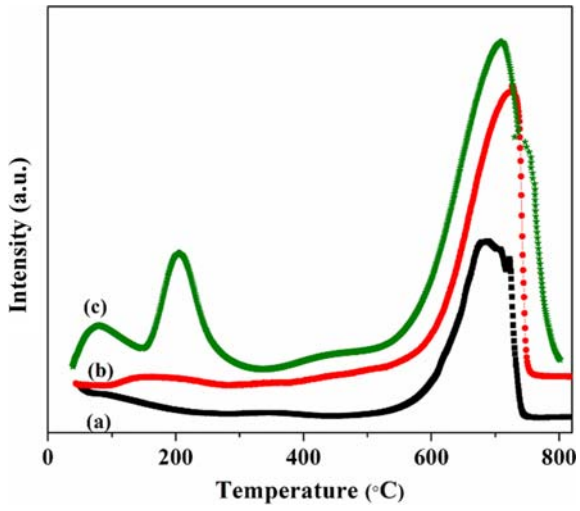

Fig. 6. TPO profiles of spent catalyst after 300 min time on stream, (a) 5% Ni/Al_2O_3, (b) 10% Ni/Al_2O_3, (c) 15% Ni/Al_2O_3, CO_2/CH_4=1, GHSV=18,000 ml/g_{cat}·h.

hydrogenated to methane even below 200 °C. It showed that carbidic C_α species is rather active and thermally unstable on nickel surface. A significant amount of surface carbon species was hydrogenated to methane below 400 °C and was assigned to partially dehydrogenated C_β species. The majority of the surface carbon was hydrogenated above 500 °C and attributed to carbidic clusters $C\gamma$.

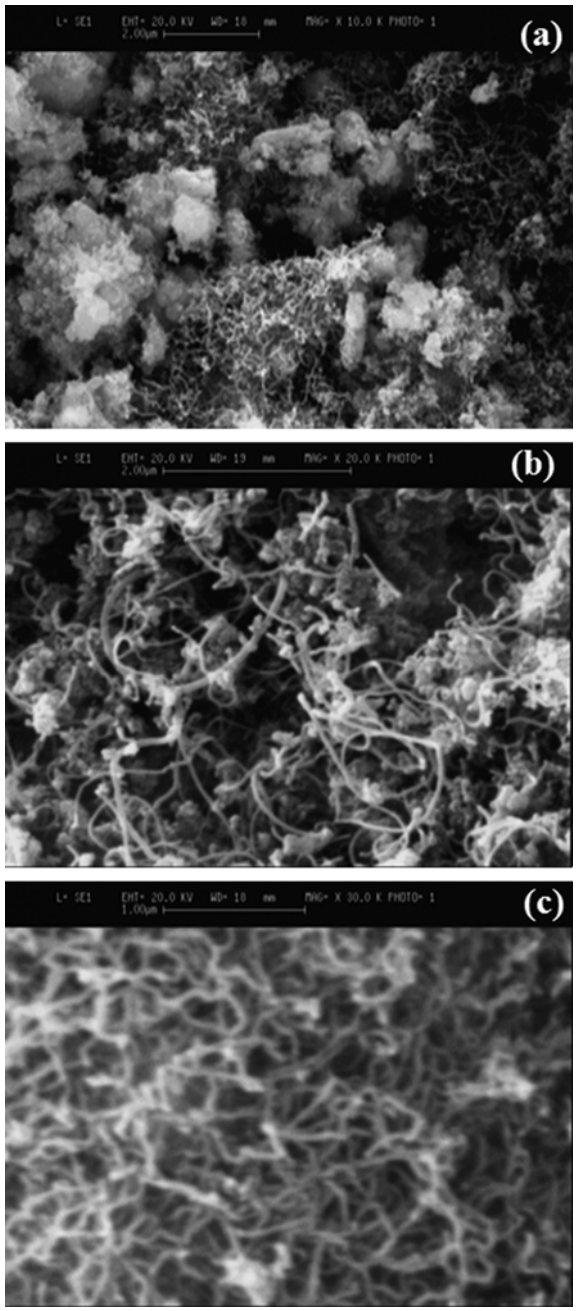

Fig. 7. SEM analysis of spent catalyst after 300 min time on stream, (a) 5% Ni/Al_2O_3, (b) 10% Ni/Al_2O_3, (c) 15% Ni/Al_2O_3, CO_2/CH_4=1, GHSV=18,000 ml/g_{cat}·h.

As can be seen in Fig. 8, the first peak at around 300 °C, might be amorphous carbon (C_β) on the nickel sites, while the second peak at above 500 °C, is identified as carbon whisker ($C\gamma$). The results show that increasing in nickel loading increased the amount of deposited carbon and also increased the fraction of amorphous and whisker carbon. These results are in agreement with those obtained from TPO and SEM analyses.

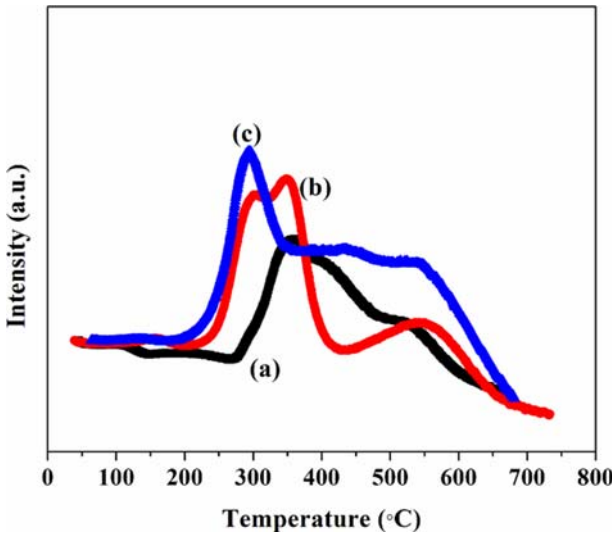

Fig. 8. TPH analysis of spent catalysts after 300 min time on stream, (a) 5% Ni/Al_2O_3, (b) 10% Ni/Al_2O_3, (c) 15% Ni/Al_2O_3, CO_2/CH_4=1, GHSV=18,000 ml/g_{cat}·h.

Table 2. Effect of CO_2/CH_4 ratio on the catalytic performance of 10% Ni/Al_2O_3 at 700 °C, GHSV=18,000 ml/g_{cat}·h

H_2/CO ratio	CO_2 conversion (%)	CH_4 conversion (%)	CO_2/CH_4 ratio
1.03	88.8	54.0	0.5
0.80	77.1	72.1	1
0.68	61.5	93.5	2
0.52	48.6	98.6	3

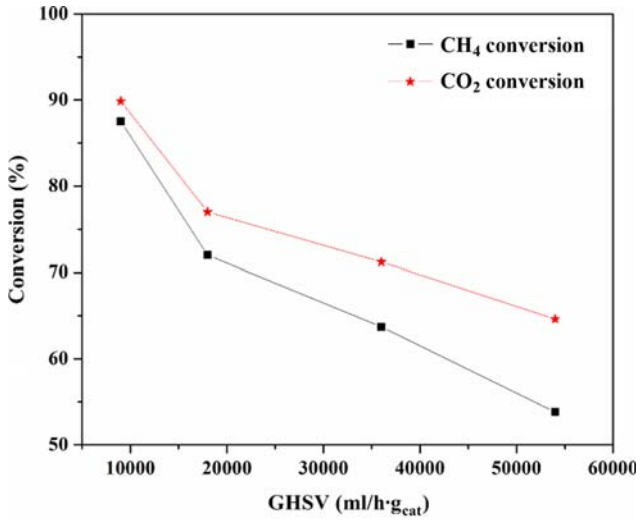

Fig. 9. Effect of GHSV on the catalytic performance of 10% Ni/Al_2O_3 at 700 °C, CO_2/CH_4=1.

The effect of feed ratio on catalytic properties over 10%Ni/Al_2O_3 is presented in Table 2. The results show that by increase of CO_2/CH_4, the methane conversion increased and the CO_2 conversion decreased. Increasing in CO_2/CH_4 ratio decreased the H_2/CO ratio because of water gas shift reaction. The water gas shift reaction (WGSR) was carried out simultaneously in the reformer. It is favorable at lower temperature and in the presence of steam, promoting H_2 production and consuming CO.

The effect of gas hour space velocity (GHSV) over 10%Ni/Al_2O_3 catalyst is shown in Fig. 9. As can be seen, the increase of GHSV decreases the conversion of methane (CH_4) and carbon dioxide (CO_2). Generally, there are two reasons for the obtained results: reforming of methane by CO_2 is an endothermic reaction, and an increase of reaction temperature increases the thermal enthalpy. To keep the conversion of reactants and yield of products constant, more thermal energy is needed at higher GHSV values. So as GHSV increases, more thermal energy is required for reforming reaction and to preheat the feed gas mixture, which finally decreases the reactants conversion.

CONCLUSIONS

Nanostructured γ-Al_2O_3 with high surface area and mesoporous structure was synthesized by sol-gel method and employed as catalyst support for nickel catalysts in methane reforming with carbon dioxide. The BET analysis showed a high surface area of 204 m^2g^{-1} and a narrow pore-size distribution centered at a diameter of 5.5 nm for catalyst support. The results revealed that increasing the nickel loading from 5 to 15 wt% decreased the surface area of catalyst from 182 to 160 m^2g^{-1}. In addition, the catalytic results showed an increase in methane conversion with increasing nickel content up to 10 wt%, and the catalyst with 10 wt% of nickel possessed the highest catalytic activity. TPO analysis revealed that the coke deposition increased with increasing nickel loading and the catalyst with 15 wt% of nickel showed the highest degree of carbon formation. Increasing CO_2/CH_4 ratio increased the methane conversion. The BET analysis of spent catalysts indicated that the mesoporous structure of catalysts still remained after reaction.

REFERENCES

1. X. Dongyan, L. Wenzhao, G. Qingjie and X. Hengyong, *Fuel Process Technol*., **86**, 995 (2005).
2. J. Juan-Juan, M. C. Roman-Martinez and M. J. Illan-Gomez, *Appl. Catal. A*., **359**, 27 (2009).
3. B. Zheng, Y. Jianhua, L. Xiaodong, C. Yong and C. Kefa, *Int. J. Hydrog. Energy*, **33**, 5545 (2008).
4. A. E. Luna and M. E. Iriarte, *Appl. Catal. A*., **343**, 10 (2008).
5. M. Rezaei, S. M. Alavi, S. Sahebdelfar and Z. F. Yan, *J Nat. Gas Chem*., **15**, 327 (2006).
6. B. Nematolahi, M. Rezaei and M. Khajenoori, *Int. J. Hydrog. Energy*, **36**, 2969 (2011).
7. E. Navaei and M. Rezaei, *Scripta Mater*., **61**, 212 (2009).
8. S. Therdthianwong, A. Therdthianwong, C. Siangchin and S. Yongprapat, *Int. J. Hydrog. Energy*, **33**, 991(2008).
9. E. Ruckenstein and H. Y. Wang, *J. Catal*., **205**, 289 (2002).
10. J. M. Rynkowski, T. Paryjczak and M. Lenik, *Appl. Catal. A*., **106**, 73 (1993).
11. H. Mori, C. Wen, J. Otomo, K. Eguchi and H. Takahashi, *Appl. Catal. A*., **245**, 79 (2003).
12. C. H. Bartholomew, *Catal. Rev. Sci. Eng*., **24**, 67 (1982).
13. C. Mirodatos, H. Praliaud and M. Primet, *J. Catal*., **107**, 275 (1987).
14. Y. G. Chen and J. Ren, *Catal. Lett*., **29**, 39 (1994).